ISSN 2070-2051, Protection of Metals and Physical Chemistry of Surfaces, 2020, Vol. 56, No. 3, pp. 651–662. © Pleiades Publishing, Ltd., 2020.

PHYSICOCHEMICAL PROBLEMS OF MATERIALS PROTECTION

Preparation, Spectral Characterization and Corrosion Inhibition Studies of (*E*)-*N*-{(Thiophene-2-yl)methylene}pyrazine-2-carboxamide Schiff Base Ligand

Festus Chioma[a], Odozi W. Nnenna[b, *], and Olakunle Moses[b]

[a] *Inorganic Unit, Department of Chemistry, Ignatius Ajuru University of Education, P.M.B. 5047 Rumuolumeni, Port Harcourt, Rivers State, Nigeria*

[b] *Physical Chemistry Unit, Department of Chemistry, University of Ibadan, Oyo State, Nigeria*

**e-mail: nw.odozi@gmail.com*

Received September 23, 2019; revised January 6, 2020; accepted January 10, 2020

Abstract—The study described the preparation and characterization of thiophene/pyrazine Schiff base, *(E)*-*N*-{(thiophene-2-yl)methylene}pyrazine-2-carboxamide (HL) using melting point and micro (CHN) analysis; vibrational, nuclear magnetic resonance (^{1}H- and ^{13}C-NMR) and electronic (UV–Vis) spectroscopies. HL was also studied for adsorption and corrosion properties. The spectral data were consistent with tridentate bonding nature and enolimine tautomeric arrangement within the ligand assemblage giving credibility to its formation. Density functional theory (DFT) calculations correlated the investigational data, while its percentage inhibition efficiency (IE, %) increased with rise in concentration though declined with increase in temperature (*T*). The latter indicate that the inhibition proficiency (IP) with *T* was mixed adsorption, with physisorption dominating the corrosion inhibition process. Similarly, the adsorption of HL on the mild steel (ms) obeys Langmuir adsorption isotherm. However, the negative sign of ΔG°_{ads} and ΔH°_{ads} designates that HL adsorption on the ms surface in 1.0 M HCl was instantaneous and exothermic correspondingly. Furthermore, the scanning electron microscopy (SEM) data corroborates that HL hinders ms corrosion through the formation of protective layers on ms surfaces.

Keywords: Schiff base, pyrazine-2-carbaldehyde, DFT, mild-steel, corrosion

DOI: 10.1134/S2070205120030107

INTRODUCTION

Mild steel (ms), a foremost material of construction is expansively adopted in chemical as well as allied industries owing to its accessibility, low cost and unfussy assemblage [1, 2]. The uses of ms spans across various industrial sectors and units including the oil and gas, chemical processing plants, automobile, etc. Largely, metals as well as their alloys display natural propensity of spontaneously reacting with their environment to acquire lesser energy by developing chemical compounds in more steady condition(s). The latter produces destructive influence on the motorized properties of the metals. Consequently, research has shown that steels and their byproducts, which are vulnerable to bout in destructive media, are the frequently exposed species in manufacturing environments [3, 4]. For prevention or retardation of metallic dissolution in addition to reduction of acid intake; corrosion inhibitors are normally adopted [5]. Compounds with amines, fatty amides, oxygen, sulphur or phosphorous moieties as surfactants have remained documented as corrosion inhibitors. Similarly, the use of carbon-based and synthetic materials as corrosion inhibitors of metals and alloys have stood extensively reported [6, 7]. Most known effective inhibitors are heterocyclic assemblages with O, N and S heteroatoms in addition to multiple bonds within their cyclic structures through which they are adsorbed on metallic surfaces by developing organic film layers [8]. Research reports [3, 5] also have it that effective adsorption often depends on basic physicochemical properties (functional moieties, electron density at the donor atom, π-orbital character and the electronic configuration) within the inhibitor structural assemblage. Effectiveness of carbon-based compounds as inhibitors remains principally reliant on their capacity to get adsorbed on metallic surfaces thus substituting aquo fragments at the oxidizing edges. Derivatives of heterocyclic assemblages have stood as the utmost operative inhibitors [9, 10] owing to the existence of N, O, S, Se plus P in forming coordinate-covalent bonds with metallic ions, a consequence of free electron pairs [11] residing on the heteroatoms. Likewise, compounds bearing π-bonds often exhibit excellent inhibitive possessions, a consequence of π-orbital interac-

tion with metallic surfaces [12]. Generally, carbon-based molecules have been accepted to inhibit corrosion through adsorption at the metallic–solution interface [13]. The mechanisms of adsorption associated with carbon-based compounds include blockage of reaction spots or creating physical barrier to lessen the diffusion of corrosive species on the metallic surfaces. In an attempt to broaden the existence of economical and environmentally friendly inhibitors, this present study report the preparation of a new thiophene/pyrazine Schiff base ligand, *N*-(thiophen-2-ylmethylene)pyrazine-2-carboxamide as a probable corrosion inhibitor.

MATERIALS

The chemicals; thiophene/pyrazine, concentrated hydrochloric acid, acetone, sodium hydroxide, zinc dust, glacial acetic acid, trimethylamine and ethylenediamine, were all delivered by Sigma-Aldrich limited as analytical reagent quality and used without any sort of distillation. The ethanol solvent was purchased as drum standards and purified using conventional techniques [14]. The ms piece was acquired from an open market in Ibadan, Oyo State, Nigeria.

METHODS

The synthesized ligand was evaluated for solubility in polar and non-polar solvents. Melting point (uncorrected) was carried out using an Electro-thermal Temp-Mel melting point device on the synthesized compound. The micro-analysis (CHN) for synthesized Schiff base was acquired on Perkin-Elmer 7300 DV and Leco, CHNS-932 elemental analyzers. The vibrational spectral data were obtained on Bruker FT/IR-4100 Billerica spectrometer as triplet scans using the KBr disc method in the 4000–350 cm^{-1}, while the electronic data were acquired amid 190–900 nm scan range by means of Lambda 25 UV/visible spectrophotometer. The ^{1}H and ^{13}C NMR spectra for the Schiff base were acquired at 301 K on Bruker DRX-400 MHz spectrophotometer in DMSO-d_6. The internal standard, tetramethylsilane (TMS) served as reference for the NMR chemical shifts.

EXPERIMENTAL

Synthesis of (E)-N-{(Thiophene-2-yl)methylene}pyrazine-2-carboxamide (HL)

The Schiff base, (*E*)-*N*-{(thiophene-2-yl)methylene}pyrazine-2-carboxamide (Scheme 1) with molecular weight, 217 g mol^{-1} was synthesized following an earlier reported procedure [15] with slight modification. An equimolar concentration of thiophene-2-carbaldehyde (0.000045 mmol, 5000 mg) and pyrazine-2-carboxamide (0.000045 mmol, 5489 mg) were liquefied in ethanol (30 mL). The mixture was catalyzed using ±3 mL of CH_3CO_2H and refluxed for 3 h on a magnetic-stirrer hotplate. Solid precipitates were acquired on ice refrigeration, filtered under gravity, recrystallized from ethyl-alcohol to afford the Schiff base dried in desiccator over silica gel. The chemical structure and nomenclature of the Schiff base was acquired using ISIS-draw as well as Chem-draw respectively. Yield: 7485 mg, MW: 217.186 g/mol, 66%. Shade: brown, m.p: 236–238°C. IR (KBr) ν/cm^{-1}: 3401 m (HC=N), 3146s (CH), 1699s (C=N), 1606 (C=C), 1434 (C=O), 1374s (C–N), 1020s (C–C), 784 δ(C–H). ^{1}H NMR (300 MHz, DMSO-d_6) δ ppm: 7.85 (s, J(0.92), 0.84, H–C=N); 8.66–8.67 (d d, J(2.58, 1.53), 1.13, 2H, $H_{5\&6}$ pyrazine); 8.23 (s, J(1.10), 0.84, 1 H, H_2 pyrazine); 8.81 (d, J(2.53), 1.14, 1H, H_{12} thiophene); 9.16 (d, J(1.53), 1.05, 1H, H_{13} thiophene); 7.94 (d, J(0.82), 1H, H_{11}). ^{13}C NMR (75 MHz, DMSO-d_6) δ ppm: 165.5 ($C_{5,6}$); 147.8 (C_9), 145.4 (C_2), 144.1 (C_7), 143.7 (C_3), 40.5 (C_{10}), 40.3 (C_{13}), 40.1 (C_{11}) and 39.9 (C_{12}). UV/visible (cm^{-1}): 35811, 36215 (π–π*), 26661, 25635 (n–π*); Anal. Calcd. for $C_{10}H_7N_3OS$ (%): C, 55.29 (55.26), H, 3.25 (3.31), N, 19.35, (19.29).

Specimen Preparations

Percentage composition of ms sample (wt %) used were 21×10^{-1}, C; 9×10^{-1}, Mn; 22×10^{-2}, P; 3×10^{-2}, Si; 30×10^{-2}, S; 11×10^{-1}, Cr; 12×10^{-1}, Ni; 22×10^{-2}, Mo; 7×10^{-2}, Al; 15×10^{-1}, Cu and Fe as the balance. The ms pieces stood mechanically pressed cut into coupons of dimension 4 cm/4 cm/0.45 mm. These coupons were used as delivered devoid of further polishing but remained degreased in ethyl-alcohol, dried in acetone, weighed and stored in a dehydrated desiccator before use [16].

Gravimetric Method

The weight loss (WL) experimentation stood completed in a 100 mL 1 M HCl solutions with several concentrations of the Schiff base ligand. Earlier weighed coupons were wholly submerged in 100 mL of the test solution. The system was maintained at 303 K. To evaluate WL, the coupons remained recovered afterward 5 h of immersion, placed in 20% sodium hydroxide solution comprising 200 gL^{-1} Zn dust, cleaned using bristle brush, washed with abundant aqueous solvent followed by acetone, dehydrated, and weighed. The variation in mass of the coupons after 5 h of submerge and its original weight were considered as the WL. The experimentations were repeated at 313, 323, 333, and 343 K temperatures. From WL values, corrosion rates (C_R) stood calculated with the formula [17].

$$C_R = \frac{m_1 - m_2}{At}. \quad (1)$$

The surface coverage (θ) and IE% which is the inhibition efficiency (IE) of HL was computed according to Eqs. (2) and (3) [18].

$$\theta = \frac{C_{R(blank)} - C_{R(inh)}}{C_{R(blank)}}, \quad (2)$$

$$IE,\% = \theta \times 100. \quad (3)$$

Surface Analysis

Morphological studies of the ms surfaces after 5 h of submerge in 1 M HCl solutions with and without 1.0 mM HL solution at 290 K stood evaluated with SEM-COATER MODEL Q150RES.

Quantum Chemical Analysis

Quantum chemical methods (QCMs) have attracted global attention in predicting the performances of corrosion inhibiting compounds [19], a consequence of the considerable role computational chemistry plays in explaining the electronic and molecular structures as well as reactivity of compounds [20]. Progressively, QCMs through DFT has remained proficiently adopted to gain better knowledge of chemical reactivity and choice of attractive site of molecular compounds. Also, in corrosion studies, it helps in the description of the nature and structure of anti-corrosion compounds [21]. Molecular descriptors like HOMO energy, LUMO energy, band gap, dipole moment and Mullikan charges offers great contributions in the assessment of molecules as corrosion inhibitors [22]. The present study adopted DFT for full optimization on the inhibitor molecule using hybrid functional Becke 3 Lee Yang Par (B3LYP) stage of theory with 6-3IG* (D) source set through Spartan 14 (Version 1.2.0) program. Various hypothetical factors like energy of highest occupied molecular orbital (E_{HOMO}), lowest unoccupied molecular orbital (E_{LUMO}), energy band gap (ΔE; $E_{LUMO}-E_{HOMO}$), electronegativity (χ), global hardness (η) and global softness (S), fraction of electron transfer (ΔN) plus dipole moment (μ) were calculated to describe the global reactivity of the HL molecule.

RESULT AND DISCUSSION

Synthesis

The 1 : 1 mole ratio reaction of thiophene-2-carbaldehyde and pyrazine-2-carboxamide in ethyl-alcohol solution afforded the pyrazine Schiff base, (*E*)-*N*-{(thiophene-2-yl)methylene}pyrazine-2-carboxamide. The acquired analytical and spectral data corroborated the structure of the synthesized ligand. The ligand was intensely colored adopting an unchanging solid nature.

Microanalysis

The microanalysis data established a 1 : 1 coordination stoichiometic ratio for the synthesized ligand. The acquired experimental figures were strongly in agreement with theoretical values and consistent with proposed chemical composition for the synthesized compound.

Spectral Studies

Critical evaluation of the ^{1}HNMR spectrum (Fig. 1) of (*E*)-*N*-{(thiophene-2-yl)methylene}pyrazine-2-carboxamide acquired in DMSO-d_6 indicates the absence of a peak typical of OH functional group often associated with thiophene-2-carbaldehyde within 20.0–15.0 ppm rather a signal around 7.85 ppm was detected. The latter results from the existence of enolimine tautomeric assemblage of the synthesized Schiff base ligand giving credibility to an aminopyarzinethiophene ligand creation. The assemblage suggested for the Schiff base ligand was substantiated by the presence of a lone resonated signal at 7.85 ppm corroborative of H–C=N moiety. The pyrazine cyclic protons were detected at 8.67 ppm as double-doublet and 8.23 ppm as a lone peak, whereas the thiophene hydrogen atoms were observed as doublet signals at 7.94 ppm, 8.81 ppm and 9.16 ppm. The spectrum (^{13}C NMR) of the Schiff base ligand (Fig. 2) revealed resonance peaks arising from the pyrazine aromatic atoms (C_2, C_3, $C_{5\&6}$) around 145.5, 143.7, and 165.5 ppm. The peaks within the sort 39.90–40.53 ppm were carefully apportioned to C_{11}, C_{12} and C_{13} atoms separately of the thiophene function. Also, detected lone signals at 147.8 and 144.1 ppm were credited to C_9 and C_7 atoms of the imine and ketonic moieties. Substantial vibrational bands were cautiously allotted on association to documented accounts of related structures [23]. The vibrational spectrum of (*E*)-*N*-{(thiophene-2-yl)methylene}pyrazine-2-carboxamide (Fig. 3) exhibited a broad-like band at 3401 cm^{-1} apportionable to intramolecular proton bonding (ν C–H...N) of an imine assemblage giving credence to Schiff base formation. The latter also confirms the dehydration of the carbanolimine to afford the Schiff base and absence of both NH and OH stretching vibrations often detected in pyrazine-2-carboxamide and thiophene-2-carbaldehyde. The absorption bands arising from the C–H function was noticed at 3146 cm^{-1}. While the imine moiety absorption band was detected at 1699 cm^{-1}, the characteristic vibration band due to C=C groups vibrated as a signal band at 1606 cm^{-1}. Also the free C=O moiety appeared a strong band at 1434 cm^{-1}. The bands at 1374, 1020, and 784 cm^{-1} in the Schiff base spectrum were ascribed to ν (C–N), ν (C–C) and δ (C–O) vibrations independently. The ligand presented intraligand bands of $\pi^* \leftarrow$ n and $\pi^* \leftarrow \pi$ only as no d–d or

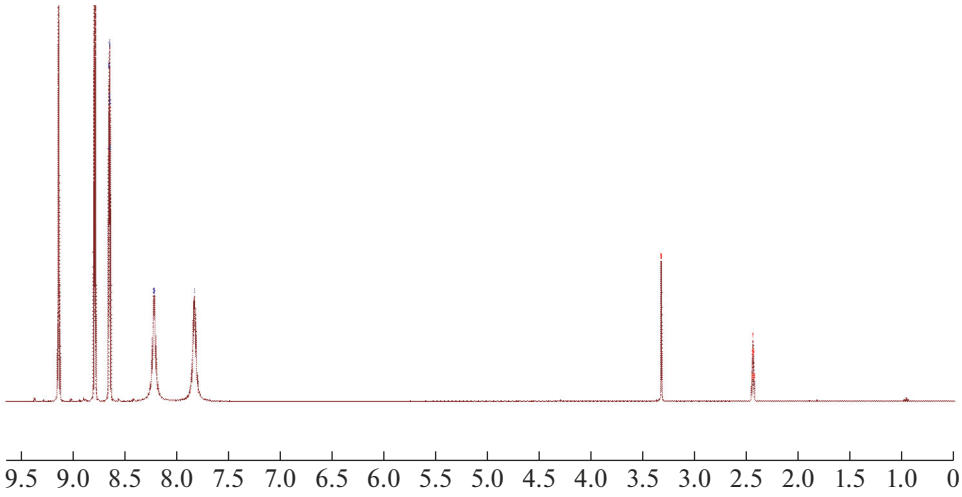

Fig. 1. ^{1}HNMR spectrum of HL ligand.

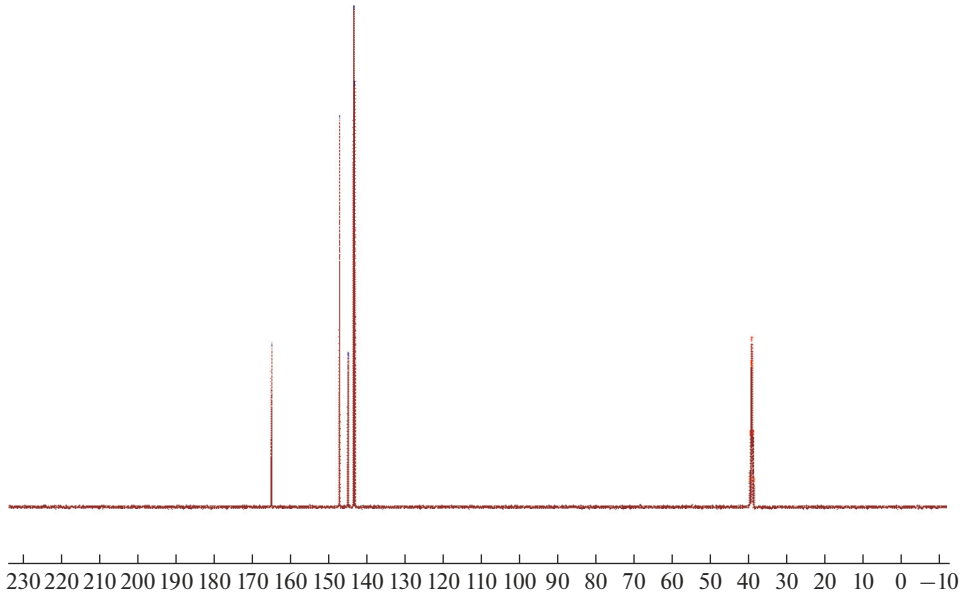

Fig. 2. ^{13}CNMR spectrum of HL ligand.

L → MCT transitions were expected in the ultraviolet region. The coupled two bands each detected in the ligand spectrum at 35811 and 36215; and 26661 and 25635 cm^{-1} were credited to π–π*and n–π* transitions within the ligand assemblage.

Weight Loss (WL) Measurement

Corrosion parameter figures like corrosion rates (C_R), IE (%) and θ contained in Table 1 were acquired from gravimetric experimentations on ms in 1 M HCl solution with and without HL at 20–100 μM concentrations and 303–343 K temperature ranges. Table 1 confirms that the high IE (94.64%) displayed by HL at optimum concentration (100 μM) and room temperature advocates additional θ of the ms surface by the inhibitor molecule [24]. The latter corroborates HL as a good corrosion inhibitor (CI) for ms in 1 M HCl solution. Figures 4 and 5 denote WL and corrosion level as a function of inhibitor concentration (IC) at various T_s, individually, whereas Figs. 6 and 7 denotes %IE as a function of concentration and T separately. The IE proliferates with rise in inhibitor concentrations and declines with rise in T_s. The proliferation in %IE with rise in HL concentrations could be due to adsorption or formation of protective films on the sur-

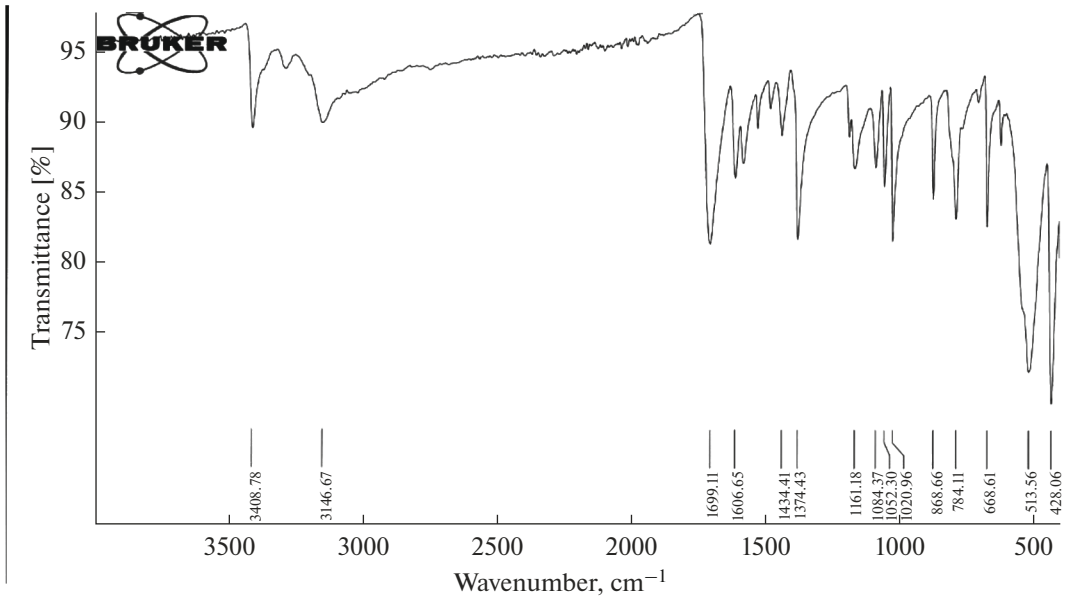

Fig. 3. FTIR spectrum of HL ligand.

face of the metal by the inhibitor, whereas the decrease in %IE at higher Ts may result from desorption of the adsorbed molecules from metallic surface. [25]

Effect of Temperature and Activation Parameters

Temperature play foremost role in ascertaining the corrosion properties of ms. The latter includes inhibitor decomposition, desorption plus rapid etching which occurs at the metallic superficial area at different Ts in the inhibitor solution [26]. The data acquired (Figs. 6 and 7) at 303–343 K temperature series portrays that C_R with and without HL improved as T was raised. The kinetics of HL action can be acquired by making a comparison of the activation parameters: E_a (activation energy), ΔH^* (enthalpy of activation) and ΔS^* (entropy of activation) with and without the inhibitor. These parameters were computed from the Arrhenius Eq. (4) and the transition state theory Eq. (5)

$$\log C_R = \log A - \frac{E_a}{2.303T}, \quad (4)$$

$$\log \frac{C_R}{T} = \left[\left(\log\left(\frac{R}{Nh}\right) + \left(\frac{\Delta S^*}{2.303R}\right)\right)\right] - \frac{\Delta H^*}{2.303RT}. \quad (5)$$

Figure 8 indicates a plot of log C_R against $1/T$ K^{-1} for ms as straight lines with slope of $(-E_a/2.303R)$ from which E_a values were computed and itemized in Table 2. The E_a with varied concentrations of HL in 1 M HCl improved compared to that acquired without the inhibitor. The improved data of E_a designate robust inhibitive activity of HL by improving energy

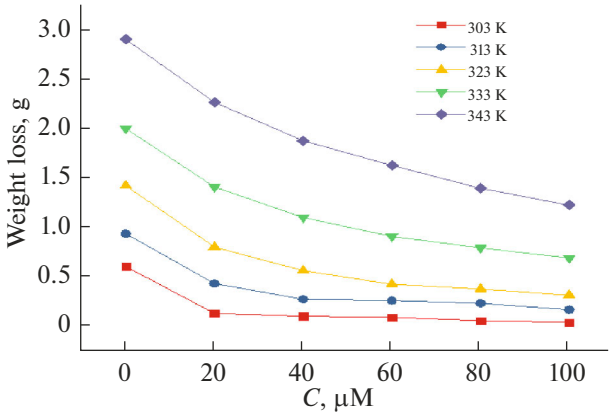

Fig. 4. Plot of a WL against IC, after 5 h of immersion at different Ts.

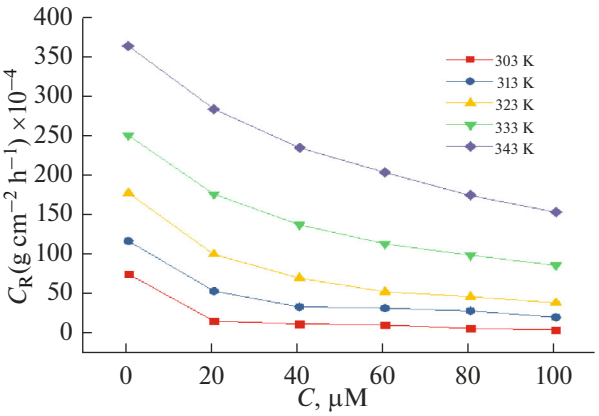

Fig. 5. Plot of a C_R against IC, after 5 h of immersion at different Ts

Table 1. Corrosion parameters from WL determinations for ms in 1 M HCl at varied Ts

Temp., K	Concentration of inhibitor, μM	WL, g	C_R (g cm^{-2} h^{-1})×10^{-4}	IE, %	θ
303	0.0	0.5968	74.60	–	–
	20	0.1217	15.21	79.61	0.796
	40	0.0925	11.56	84.50	0.845
	60	0.0818	10.23	86.29	0.863
	80	0.0476	5.95	92.02	0.920
	100	0.0320	4.00	94.64	0.946
313	0.0	0.9298	116.23	–	–
	20	0.4239	52.99	54.41	0.544
	40	0.2650	33.13	71.50	0.715
	60	0.2520	31.50	72.90	0.729
	80	0.2241	28.01	75.90	0.759
	100	0.1589	19.86	82.91	0.829
323	0.0	1.4144	176.80	–	–
	20	0.7951	99.39	43.79	0.438
	40	0.5550	69.38	60.76	0.608
	60	0.4172	52.15	70.50	0.705
	80	0.3677	45.96	74.00	0.740
	100	0.3053	38.16	78.41	0.784
333	0.0	1.9952	249.40	–	–
	20	1.4026	175.33	29.70	0.297
	40	1.0944	136.80	45.15	0.452
	60	0.9018	112.73	54.80	0.548
	80	0.7861	98.26	60.60	0.606
	100	0.6828	85.35	65.78	0.658
343	0.0	2.8993	362.40	–	–
	20	2.2615	282.70	22.00	0.220
	40	1.8711	233.89	35.46	0.355
	60	1.6221	202.76	44.05	0.441
	80	1.3890	173.63	52.09	0.521
	100	1.2192	152.40	57.95	0.580

C_R = corrosion rate; %IE = inhibition efficiency; θ = surface coverage; T = temperatures.

hindrance for the metallic corrosion process [27]. The decline in IEs with increased T and the rise in E_a with the inhibitors shows physical adsorption of inhibitor molecules on the metallic surface [28]. The physical adsorption of the inhibitor on the metallic surface affords formation of physical blockade amid the metallic surface, similarly obstructing charge transfer hence retarding the metallic reactivity in corrosive electrochemical reactions [29]. To acquire additional facts about corrosion process, activation kinetic factors like ΔH^* and ΔS^* were evaluated using transition state Eq. (5) [30].

Figure 9 denotes a linear scheme of log C_R/T against $1/T$ K^{-1} through an intercept of log (R/Nh) + (ΔS^*/2.303), a straight line through a slope of $\Delta H^*/2.303R$ and used to evaluate the data of ΔH^* and ΔS^* as summarized in Table 2. The ΔH^* displayed

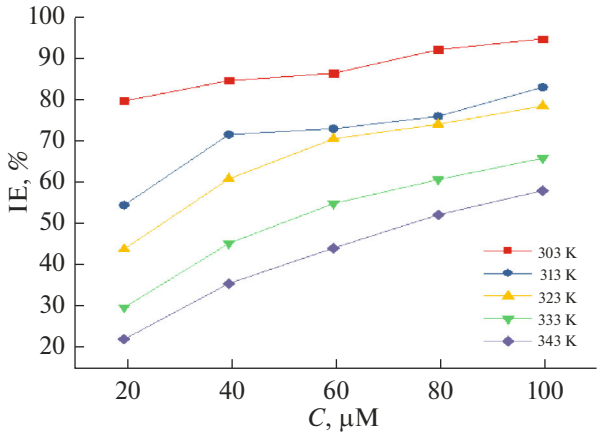

Fig. 6. Plot of IE (%) against IC at different Ts.

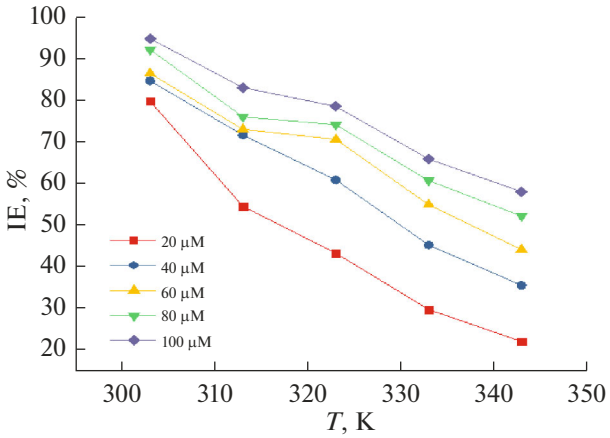

Fig. 7. Plot of IE (%) against T at different ICs.

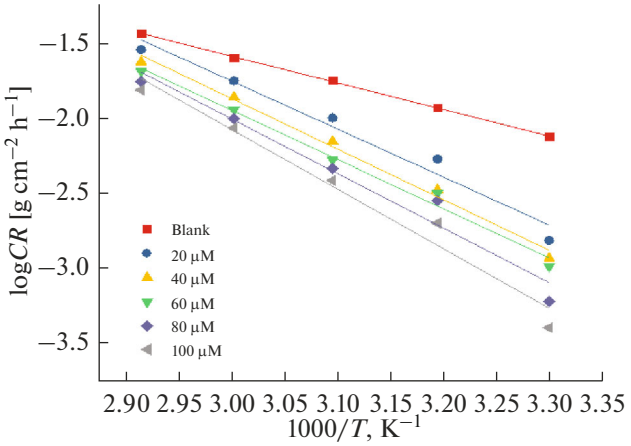

Fig. 8. Arrhenius scheme of ms corrosion in 1 M HCl solution of HL ligand at varied concentrations.

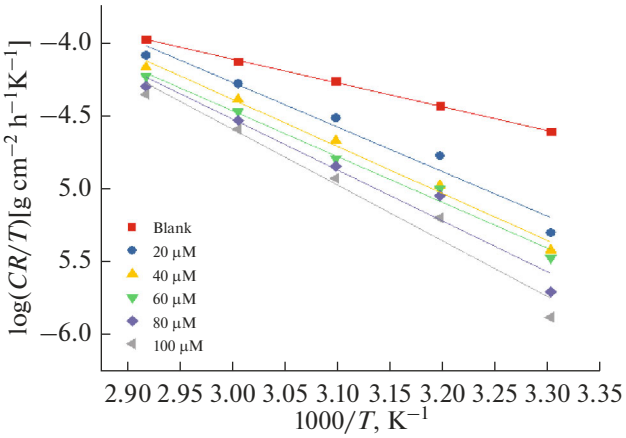

Fig. 9. Transition state plots for ms corrosoin 1 M HCl solution of HL ligand at varied Ts.

comparable trend like the precursor Ea data i.e. data proliferates as IC raised. The positive sign of the enthalpies of activation reveal the endothermic nature of dissolution process of ms in acidic medium (Verma et al., 2017). The ΔS^* data was more negative without the inhibitor than with the inhibitor, signifying that the activated complex is more ordered in uninhibited solution. Large and negative data acquired for entropies of activation similarly submits that activated complex in the rate ascertaining step denotes an associa-

Table 2. Activation parameters of ms corrosion in varied concentrations of HL in 1 M HCl

Concentration of inhibitor, μM	E_a, kJ mol^{-1}	ΔH^*, kJ mol^{-1}	$-\Delta S^*$, kJ mol^{-1}
0	33.96	31.28	182.51
20	61.24	58.57	103.78
40	64.48	61.81	96.28
60	62.83	60.26	102.73
80	69.57	66.89	83.62
100	75.98	73.31	65.71

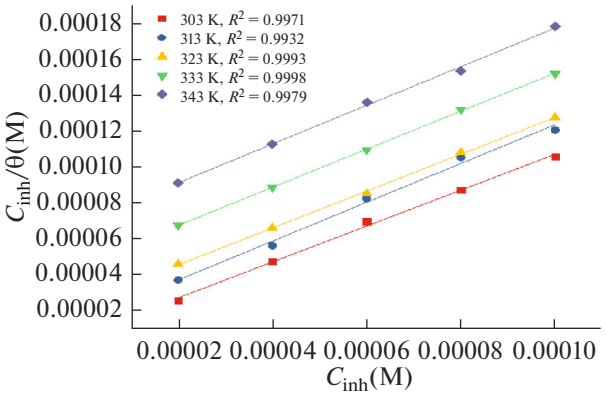

Fig. 10. Langmuir adsorption plots for ms in 1 M HCl at varied Ts with numerous concentrations of HL.

tion rather than a dissociation step, i.e. a reduction in disordering occurs on going from reactants to the activated complex [31].

3 ADSORPTION AND THERMODYNAMIC STUDIES

The adsorption isotherm (I_a) is often evaluated if inhibition influence is a function of adsorption at the metallic interface. The proficiency of heterocyclic assemblages as corrosion inhibitor resides on their adsorption on the ms surface [32]. In acid corrosion, it is anticipated that inhibitors would act through a process of adsorption on metallic surface. Adsorption of inhibitors may ascertain a structural charge of the dual layer, thus decreasing the rate of electrochemical partial reactions. Furthermore, adsorption that principally occurs at the active sites of the metallic surface may hinder the reactivity of the metal in the process of dissolution. Conversely, if the adsorption is followed by hydration, reduction or polymerization reactions of the inhibitor, thick layers could be formed thereby rendering true physical barrier. The fractional θ data were fitted into altered I_a models to acquire the required isotherm. In this present study, Langmuir I_a Eq. (6) was found to provide the best fit with correlation coefficients (R^2) close to one (>0.99) [33].

$$\frac{C_{inh}}{\theta} = \frac{1}{K_{ads}} + C_{inh}. \quad (6)$$

The plot of C_{inh}/θ versus C_{inh} afforded a straight line (Fig. 10) scheme. The figures of the slopes specify that the adsorption of HL on ms surface agrees with Langmuir isotherm. The intercept was applied to evaluate the K_{ads}, and the adsorption free energy (ΔG_{ads}) was assessed using Eq. (7). The determined figures of ΔG°_{ads} are tabulated in Table 3

$$\Delta G^{\circ}_{ads} = -RT\ln\left(K_{ads} \times 55.5\right). \quad (7)$$

Negative data resulting from ΔG°_{ads} signifies effectiveness of the adsorption process as well as steadiness of the adsorbed layer on the steel surface. Largely, ΔG°_{ads} data lesser than −20 kJ mol^{-1} often designate physisorption while higher data corroborates chemisorptions [34]. This ΔG°_{ads} values (−38.75 kJ mol^{-1} to −40.13 kJ mol^{-1}) acquired for this study were greater than −20 kJ mol^{-1}. The latter indicates that interaction of HL inhibitor with the steel surface occurs through physical and chemical adsorption [35] processes. Solmaz et al. [36], asserts that the physisorption could be the initial stage of adsorption route. The enthalpy of adsorption (ΔH°_{ads}) was acquired from Gibss–Helmholtz Eq. (8)

$$\Delta G^{\circ}_{ads} = \Delta H^{\circ}_{ads} - T\Delta S^{\circ}_{ads}. \quad (8)$$

Plot of ΔG°_{ads} against T (Fig. 11) gave the ΔH°_{ads} and standard entropy (ΔS°_{ads}). The positive values of ΔS°_{ads} in Table 4 indicates that disordering takes places when the inhibitor gets adsorbed on the metallic surface. Basically, negative figures of the $\Delta H^{\circ}_{ads} < 0$ designates exothermic process involving physisorption or chemisorption while positive values ($\Delta H^{\circ}_{ads} > 0$) corroborates endothermic processes through chemisorption. Martinez et al. [37] documented standard enthalpy of physisorption processes as −41.86 kJ mol^{-1}, whereas chemisorption processes data stood at −100 kJ mol^{-1}. Our ΔH^{o}_{ads} data was found to be −50.01 kJ mol^{-1}; but-

Table 3. Adsorption parameters from Langmuir I_a for ms corrosion in 1.0 M HCl at varied Ts

Temp., K	$-\Delta G^{\circ}_{ads}$, kJ mol^{-1}	$K_{ads} \times 10^3$, L/mol	Slope	R^2
303	40.13	149.165	1.00	0.9971
313	39.34	66.365	1.09	0.9932
323	39.29	40.659	1.03	0.9993
333	38.77	21.729	1.06	0.9998
343	38.75	14.389	1.08	0.9979

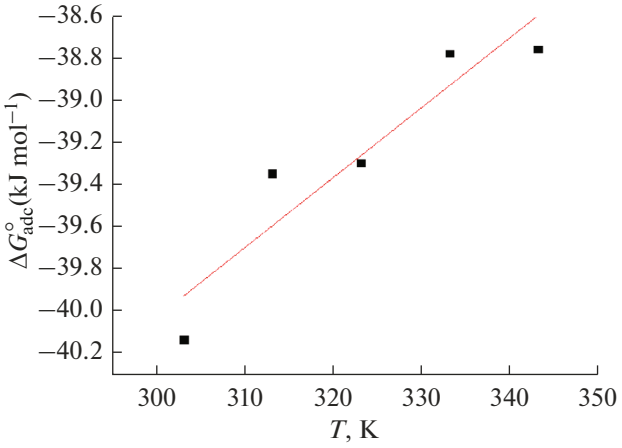

Fig. 11. A plot of ΔG^{o}_{ads} against T for corrosion inhibition ms in 1 M HCl at different Ts.

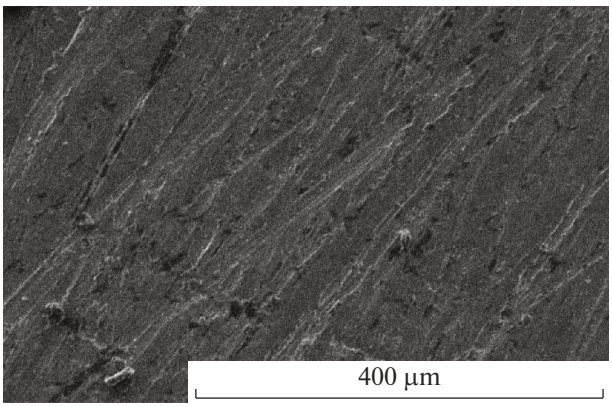

Fig. 12. SEM image of ms coupon.

tressing the fact that adsorption of HL on ms consist of mixed adsorption.

Surface Morphological Examination

Morphological studies of the ms surfaces after 6 h of immersion in 1.0 M HCl solutions of HL at 301 K were appraised using SEM. Figure 12 denotes superficial morphology of polished ms coupon that displayed uniform and consistent superficial area, while Figs. 13 and 14 shows surface imageries of ms sample with and without HL individually. In the uninhibited solution (Fig. 13), a crack and rough surface was observed including pit owing to acid corrosion, while smooth sample surface was obtained in the presence of HL (Fig. 14). Critical scrutiny of Fig. 14 indicates slight proof of existence of adsorption film corroborating adsorption of HL on ms surface through the formation of protective film.

Quantum Chemical Analysis

Density functional theory (DFT) was adopted to acquire HL structure. The optimized structure, E_{LUMO}, E_{HOMO} and electrostatic potential map of HL are presented as Figs. 15–18 respectively. The usage of frontier molecular energies to forecast electron-donating capacity of an inhibitor (i.e E_{HOMO}), the propensity to accept electron (i.e E_{LUMO}) and to ascertain reaction processes (i.e energy band gap), have been described [7]. Largely, the greater the value of E_{HOMO}, the better the propensity of an inhibitor to give-out electron [38]. Conversely, the lesser value of E_{LUMO}, signifies better propensity of an inhibitor to accept electron whereas the energy gap signifies stiffness or softness of a molecule. All evaluated frontier molecular orbital (FMO) properties for HL are displayed in Table 5. Greater values of E_{HOMO} (−6.72 eV) designates enhanced electron donating capacity of HL to suitable acceptor molecules and accordingly, better adsorption potentials of HL on the metallic surface. Lesser E_{LUMO} value (−2.72 eV) of HL molecule ascertains its ability to accept electrons. A lower energy gap (4.00 eV) amid E_{HOMO} and E_{LUMO} infers that transfer of electrons from HOMO to LUMO requires low energy that will lead to increased chemical reactions and enhanced adsorption ability [39]. Figure 18 shows that the O1 and N3 are the heteroatoms responsible for the corrosion inhibitive property displayed by HL on the ms.

Table 4. Thermodynamic parameter for the adsorption of HL on ms surface in 1.0 M HCl

Temperature, K	$K_{ads} \times 10^3$, L/mol	$-\Delta G^{\circ}_{ads}$, kJ mol^{-1}	$-\Delta H^{\circ}_{ads}$, kJ mol^{-1}	$-\Delta S^{\circ}_{ads}$, J mol^{-1}K^{-1}
303	149.165	40.13	50.01	33.30
313	66.365	39.34		
323	40.659	39.29		
333	21.729	38.77		
343	14.389	38.75		

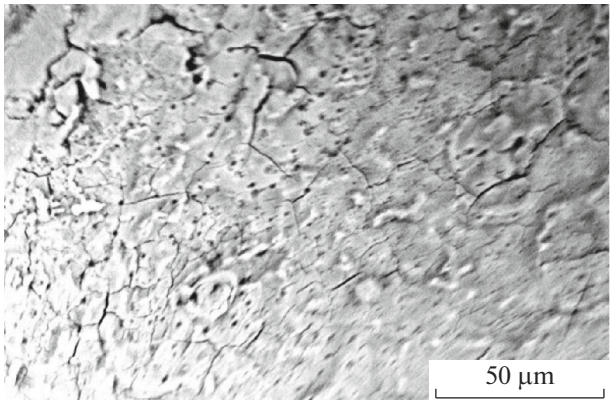

Fig. 13. SEM image for ms in 1 M HCl solution without HL ligand.

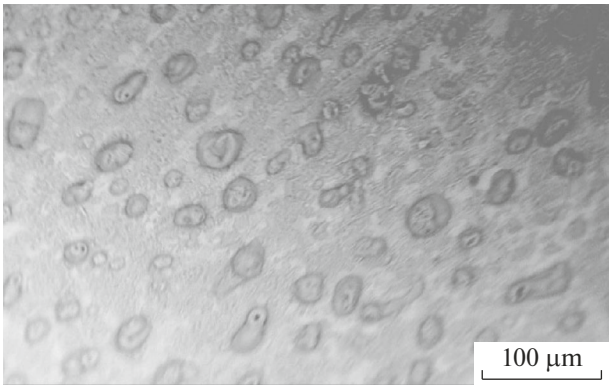

Fig. 14. SEM image for ms in 1 M HCl solution with HL ligand.

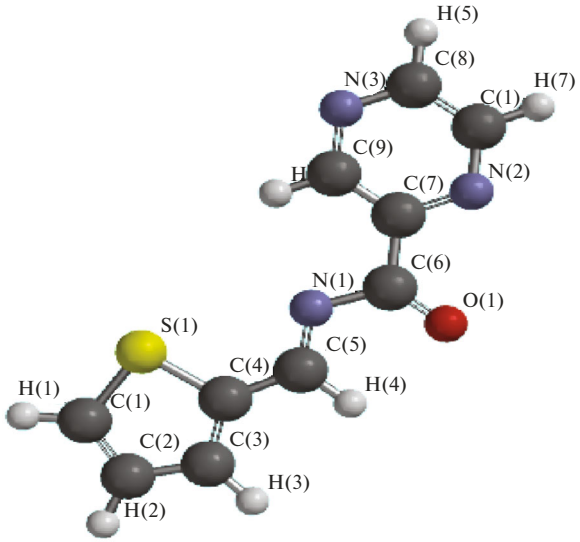

Fig. 15. Optimized structure of HL.

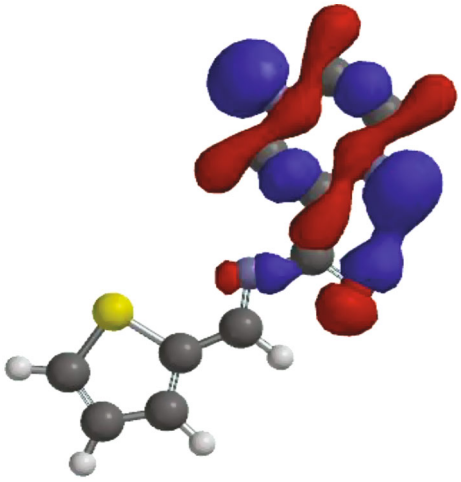

Fig. 16. FMO Diagram (HOMO) of HL ligand.

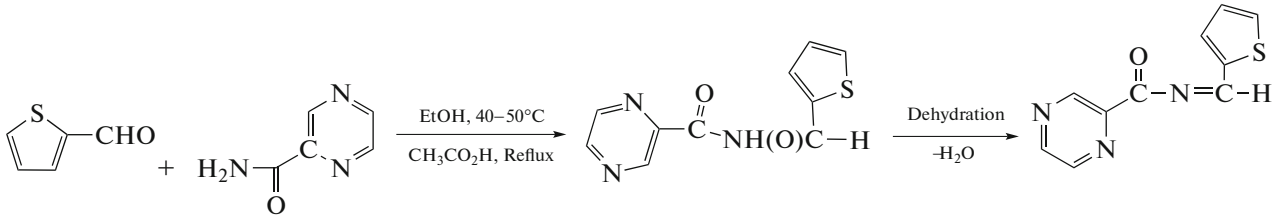

Scheme 1. Chemical structure of the Schiff Base Ligand.

CONCLUSIONS

The ligand, HL was synthesized through a condensation reflux reaction of thiophene-2-carbaldehyde and pyrazine-2-carboxamide in ethyl-alcohol solution. Investigational studies revealed tridentate (N, O, S) donor atoms and enolimine tautomeric arrangement within the ligand assemblage giving credibility to its formation. Quantum chemical calculations suggested an excellent correlation with the studied experimental results. The %IE of HL increases with rise in concentration however declines with increase in *T*.

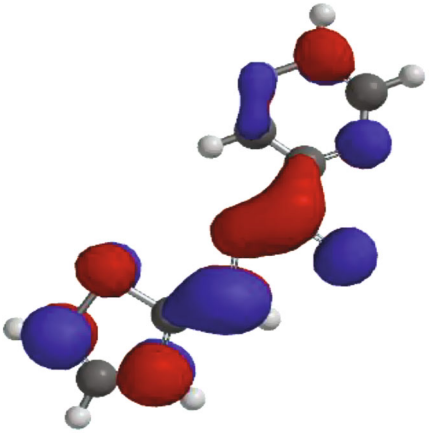

Fig. 17. FMO Diagram (LUMO) of HL ligand.

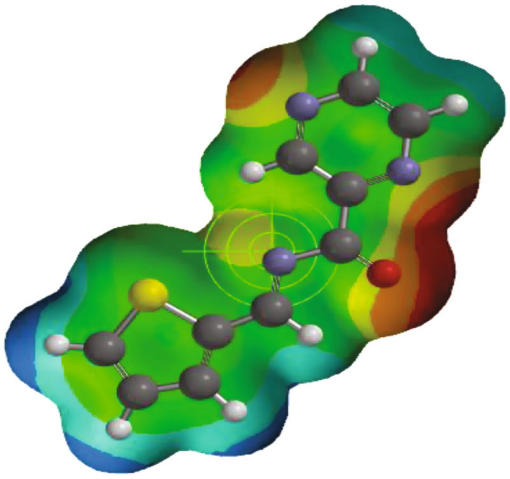

Fig. 18. Electrostatic potential map of HL ligand.

The latter indicate that the IE with temperature, kinetic factors and activation parameters for the corrosion inhibition processes is a mixed adsorption with physisorption dominating the process. Also, the adsorption of HL on the ms conforms to Langmuir adsorption isotherm. However, the negative sign of ΔG°_{ads} and ΔH°_{ads} designates that adsorption of HL on the ms surface in 1.0 M HCl was instantaneous and exothermic. Similarly, acquired SEM results confirm that HL molecule hinders ms corrosion through formation of protective layers on ms surfaces.

ACKNOWLEDGMENTS

The authors acknowledge Ignatius Ajuru University of Education, Rivers State for providing the necessary research environment for the synthesis of the compound reported in this article, and also Dr. Steve Egwuonwu who provided the grant for the purchase of the Spartan 14 software used for the computational aspect of this research work.

Table 5. Quantum chemical parameters for HL ligand

Molecular parameter	Calculated value
E_{HOMO}, eV	−6.72
E_{LUMO}, eV	−2.72
ΔE, eV	4.00
I	6.72
A	2.72
χ	4.72
η	2.00
S	0.5
ΔN	0.57
μ (D)	3.74
W	1.18

CONFLICT OF INTEREST

The authors declare that that they have no conflicts of interest.

REFERENCES

1. Melchers, R.E. and Jeffrey, R., *Corros. Sci.,* 2005, vol. 47, p. 1678.
2. Singh, A., Ebenso, E.E., and Quraishi, M.A., *Int. J. Electrochem. Sci.,* 2012, vol. 7, p. 4766.
3. Khaled, K.F., *Appl. Surf. Sci.,* 2006, vol. 252, p. 4120.
4. Afolabi, A.S., *Leonardo Electron. J. Pract. Technol.,* 2007, vol. 11 p. 143.
5. Chetouani, A., Hammoutia, B., Aouniti, A., Benchat, N., and Benhadda, T., *Prog. Org. Coat.,* 2002, vol. 45, p. 373.
6. Znini, M., Bouklah, M., Majidi, L., Kharchouf, S., Aouniti, A., Bouyanzer, A., and Hammouti, B., *Int. J. Electrochem. Sci.,* 2011, vol. 6, p. 691.
7. Odozi, N.W., Babalola, J.O., Ituen, E.B., and Eseola, A.O., *Am. J. Phys. Chem.,* 2015, vol. 4, no. 1, p. 1.
8. Khaled, K.F. and Hackerman, N., *Electrochim. Acta,* 2004, vol. 49, p. 485.
9. Hosseini, S., Azimi, A., Salari, M., and Sheikhshoaei, I., *J. Iran. Chem. Soc.,* 2010, vol. 7, p. 799.
10. Rani, B.E.A. and Basu, B.B.J., *Int. J. Corros.,* 2011, vol. 2, p. 1.
11. Adel, S.B., Deshpande, M.N., and Kolhatkar, D.G., *J. Chem. Pharm. Res.,* 2012, vol. 4, no. 2, p. 1033.
12. Ebenso, E.E., Eddy, N.O., and Odiongenyi, A.O., *Afr. J. Pure Appl. Chem.,* 2008, vol. 4, no. 11 p. 107.

13. Quartarone, G., Battilana, M., Bonaldo, L., and Tortato, T., *Corros. Sci.,* 2008, vol. 50, p. 3467.
14. Mendham, J., Denney, R.C., Barnes, J., and Thomas, M., *Vogel's Textbook of Quantitative Chemical Analysis,* New Delhi: Pearson Education Ltd., 2000.
15. Festus, C., Anthony, C.E., Osowole, A.A., Okafor, S.N., Ibeji, C.U., Onwudiwe, D.C., and Oguejiofo, T.U., *Open Chem.,* 2018, vol. 16, p. 184.
16. Obot, I.B., Obi-Egbedi, N.O., and Umoren, S.A., *Pharma Chem.,* 2009, vol. 1, no. 1 p. 151.
17. Quraishi, M. and Shukla, S., *Mater. Chem. Phys.,* 2009, vol. 113, p. 685.
18. Qu, Q., Jiang, S., Li, L., Bai, W., and Zhou, J., *Corros. Sci.,* 2008, vol. 50, p. 35.
19. Oyebamiji, A.K., Lasisi, B.M., Oyebamiji, E.O., Badegoke, A.K., Semire, B., and Adeleke, B.B., *Int. J. Mod. Chem.,* 2018, vol. 10, no. 2, p. 138.
20. Kraka, E. and Cremer, D., *J. Am. Chem. Soc.,* 2000, vol. 122, p. 8245.
21. Zarrouk, A., Hammouti, B., Lakhlifi, T., Traisnel, M., Vezin, H., and Bentiss, F., *Corros. Sci.,* 2015, vol. 90, p. 572.
22. Kaya, S. and Kaya, C., *Mol. Phys.,* 2015, vol. 113, p. 1311.
23. Małgorzata, O., Agnieszka, C., Aleksandra, K., Rafał, B., Katarzyna, T., Dorota, L., Dawid, N., and Mariusz, M., *RSC Adv.,* 2016, vol. 6, p. 52009.
24. Singh, A.K., Khan, S., Singh, A., Quraishi, S.M., Quraishi, M.A., and Ebenso, E.E., *Res. Chem. Intermed.,* 2013, vol. 39, p. 1191.
25. Li, W.H., He, Q., Zhang, S.T., Pei, C.L., and Hou, B.R., *J. Appl. Electrochem. Soc.,* 2008, vol. 113, p. 677.
26. Verma, D.K., Khan, F., Verma, C., Susai, R., and Quraishi, M.A., *Eur. Chem. Bull.,* 2017, vol. 6, no. 1, p. 21.
27. Noor, E.A. and Al-Moubaraki, A.H., *Mater. Chem. Phys.,* 2008, vol. 110, p. 145.
28. Kumari, P.P., Rao, S.A., and Shetty, P., *Procedia Mater. Sci.,* 2014, vol. 5, p. 499.
29. Szauer, T. and Brandt, A., *Electrochim. Acta,* 1981, vol. 26, p. 1257.
30. Prathibha, B.S.P., Kotteeswaran, V., and Bheema, R., *IOSR J. Appl. Chem.,* 2012, vol. 2, no. 5, p. 61.
31. Bentiss, F., Lebrini, M., and Lagrenee, M., *Corros. Sci.,* 2005, vol. 47, p. 2915.
32. Khadraoui, A., Khelifa, A., Hamitouche, H., and Mehdaoui, R., *Res. Chem. Intermed.,* 2014, vol. 40, p. 961.
33. Kumar, R., Chahal, S., Kumar, S., Lata, S., Lgaz, H., Salghi, R., and Jodeh, S., *J. Mol. Liq.,* 2017, vol. 243, p. 439.
34. Shokry, H. and Mabrouk, E.M., *Arabian J. Chem.,* 2017, vol. 10, p. S3402.
35. Lgaz, H., Salghi, R., Chaouiki, A., Shubhalaxmi, Jodeh, S., and Bhat, K.S., *Cogent Eng.,* 2018, vol. 5, p. 1441585.
36. Solmaz, R., Mert, M.E., Kardaş, G., Yazici, B., and Erbıl, M., *Acta Phys. - Chim. Sin.,* 2008, vol. 24, p. 1185.
37. Martinez, S., Valek, L., *Stipanović*, O.I., *J. Electrochem. Soc.*, 2007, vol. 154, p. 671.
38. Eddy, N.O., *Mol. Simul.,* 2010, vol. 36, p. 354.
39. Verma, C., Quraishi, M.A., and Ebenso, E.E., *Anal. Bioanal. Electrochem.,* 2018, vol. 10, p. 98.